

## REVIEW

# A review on the applied techniques of exhaled airflow and droplets characterization

Khansa Mahjoub Mohammed Merghani<sup>1</sup>  | Benoit Sagot<sup>2</sup> | Evelyne Gehin<sup>1</sup> | Guillaume Da<sup>1</sup> | Charles Motzkus<sup>3</sup>

<sup>1</sup>Univ Paris Est Creteil, CERTES, Creteil, France

<sup>2</sup>ESTACA, Montigny-le-Bretonneux, France

<sup>3</sup>CSTB, Marne-la-Vallée, France

## Correspondence

Khansa Mahjoub Mohammed Merghani, Univ Paris Est Creteil, CERTES, F-94010 Creteil, France.

Emails: khansa.mahjoub-mohammed-merghani@u-pec.fr

## Funding information

Centre Scientifique et Technique du Bâtiment

## Abstract

In the last two decades, multidisciplinary research teams worked on developing a comprehensive understanding of the transmission mechanisms of airborne diseases. This article reviews the experimental studies on the characterization of the exhaled airflow and the droplets, comparing the measured parameters, the advantages, and the limitations of each technique. To characterize the airflow field, the global flow-field techniques—high-speed photography, schlieren photography, and PIV—are applied to visualize the shape and propagation of the exhaled airflow and its interaction with the ambient air, while the pointwise measurements provide quantitative measurements of the velocity, flow rate, humidity and temperature at a single point in the flow field. For the exhaled droplets, intrusive techniques are used to characterize the size distribution and concentration of the droplets' dry residues while non-intrusive techniques can measure the droplet size and velocity at different locations in the flow field. The evolution of droplets' size and velocity away from the source has not yet been thoroughly experimentally investigated. Besides, there is a lack of information about the temperature and humidity fields composed by the interaction of the exhaled airflow and the ambient air.

## KEYWORDS

dry residues, exhaled airflow, experimental techniques, flow-field characterization, particle-laden flows, respiratory droplets

## 1 | INTRODUCTION

Morawska and Milton<sup>1</sup> recently published a commentary to the international community titled “It Is Time to Address Airborne Transmission of COVID-19”. This statement which was supported by 239 scientists confirms that breathing, speaking, and coughing generate sufficient amount of small droplets to travel further than 2 m from the source. Likewise, in a systematic literature review by Bahl et al<sup>2</sup> eight analyzed articles (out of ten) concluded that the exhaled droplets could travel horizontally for more than 2m from the source. In addition to that, a retrospective analysis on

infection transmission between three families in a Chinese restaurant confirmed the hypothesis of long-distance transmission of COVID-19.<sup>3</sup> The epidemiological data of this analysis showed that 10 subjects seated in three neighboring tables were infected, although the video record showed no close contact or fomite contact. Another analysis<sup>4</sup> of a superspreading event of COVID-19 in a choral rehearsal confirms the likability of this airborne transmission mode. In this event, 53 members out of 61 confirmed or strongly suspected to have contracted COVID-19. Moreover, cases of COVID19 spread in family clusters<sup>5-7</sup> and among healthcare staff<sup>8</sup> in close contact with patients are associated with droplet

transmission. Ong et al<sup>9</sup> detected the presence of COVID-19 virus in a patient's room, and all the tested samples were contaminated with the virus. According to Doremalen et al,<sup>10</sup> the virus remains viable for 4-72 hours on surfaces. The relative contribution of these transmission modes to the spread of the epidemic is still a controversial issue.

Special attention has been paid to the transmission mechanisms of the airborne pathogens after the emergence of novel airborne diseases, such as SARS in 2003 and H1N1 influenza in 2009. Thus, researchers in the fields of aerosol science, indoor air quality and public health conducted experimental, numerical, and theoretical studies to analyze the transport of the exhaled droplets responsible for the transmission of such diseases. The exhaled droplets are formed by the shear force caused by the passage of the airflow in the respiratory tracts while coughing, sneezing, breathing, and speaking.<sup>11</sup> These droplets vary in size and in composition which depend on their origin in the respiratory tracts.<sup>11</sup> In the case of a respiratory tract infection, the droplets carry the infectious pathogens from the tract of the infected subject and possibly transmit those to healthy individuals. Therefore, transmission can occur through three different modes of transmission. The first mode occurs via direct contact with the surface-deposited respiratory secretions of the infected person. In the second mode, the infection transmission occurs when respiratory droplets carrying infectious pathogens travel directly from the respiratory tract of the infectious individual to susceptible mucosal surfaces of the recipient.<sup>12</sup> The third mode corresponds to long-distance travel of the dry residues which results from the evaporation of the droplets. Such dry residues can transmit the infection between two individuals "who have not had face-to-face contact or been in the same room".<sup>12</sup> The relative importance of each of these modes depends on the motion and evaporation of the exhaled droplets. Therefore, the prediction of their motion and evaporation in an air jet, which requires a relevant/good coupling with humidity, temperature, and velocity fields, remains a challenging issue. The structure of humidity, temperature, and velocity fields depend on the complex interaction between the human environment (namely exhaled and inhalation airflows, human body plume) and the room surrounding environment.<sup>13</sup> Considering this complex interaction, experimental studies from the literature can be classified into two main categories which depend on the scope of the study. The first category corresponds to studies focusing on the movement and evaporation of the exhaled droplets in the human microenvironment. While the second category includes the numerical and experimental studies that consider the ventilation systems at the room scale and investigating its influence on the droplet dispersion. This review focuses on the first category and analyzes the experimental techniques applied for the characterization of exhaled airflows and droplets. The first part of this review is dedicated to the measurement systems involved in the exploration of the

### Practical implications

- This literature review discusses the applied experimental techniques and how these techniques are relevant to the characterization of the exhaled airflow.
- The article analyzes the techniques applied to determine the initial size distribution of the exhaled droplets, the evaporation process, and the size distribution of the resulting dry residues.
- Future experimental investigations of the interaction between exhaled droplets and the surrounding airflow and droplet evaporation would provide a comprehensive understanding of the host-to-host infection transmission and ultimately assess the different transmission routes.

gaseous exhaled flow, while the second part concerns the techniques applied to respiratory droplets.

## 2 | CHARACTERIZATION OF THE EXHALED AIRFLOW

This section reviews the published papers concerning the applied measurement techniques used to characterize exhalation flows while breathing, sneezing, coughing, and speaking. Here, we have identified the most relevant articles and separated them, technical-wise, into two main categories as follows: global flow-field measurements and pointwise measurements. Table 1 shows the corresponding articles and the main parameters measured. It is important to note that such parameters strongly depend on the adopted technique, and ultimately results are difficult to compare. In the following subsections, we provide an analysis of these applied techniques and discuss their pros and cons.

### 2.1 | Global flow-field measurements

The global flow-field measurement techniques provide information regarding the flow properties over the whole flow field. The global flow-field techniques and the pointwise techniques are often complementary. Global flow-field measurements provide a global information on the propagation of the exhaled jet and its interaction with the indoor airflow. As for the characterization of the exhaled flow, three global flow-field techniques are used in the literature: high-speed photography, schlieren photography, and Particle Image Velocimetry (PIV). The first two techniques which visualize the flow provide information about the flow shape, its direction, and its propagation. The propagation of the flow in the surrounding environment is usually described by two parameters,

TABLE 1 The main measured parameters of the experimental studies on the characterization of human exhaled airflow

Measurement techniques	Article	Main findings					No. of subjects		
		Measured parameters	Breathing	Coughing	Sneezing	Speaking			
Global flow field	High-speed visualization	Bourouiba et al <sup>20</sup>	Duration (ms)		300	200		1	
			Re		10 000	40 000			
			Entrainment coef. (jet phase)		0.24 ± 0.02	0.13 ± 0.02			
			Entrainment coef. (puff phase)		0.132 ± 0.06	0.055 ± 0.01			
Schlieren photography	Gupta et al <sup>15</sup>	Nose opening area (cm <sup>2</sup> )	F: 1.16 ± 0.67					5	
			M: 1.20 ± 0.52						
	Gupta et al <sup>14</sup>	Mouth opening area (cm <sup>2</sup> )	F: 0.56 ± 0.10				F: 1.80 ± 0.03	5	
			M: 0.71 ± 0.23				M: 1.80 ± 0.03		
	Schlieren photography	Xu et al <sup>16</sup>	Mouth opening area (cm <sup>2</sup> )		F: 3.37 ± 1.40				5
					M: 4.00 ± 0.95				
		Tang et al <sup>23</sup>	Propagation distance (m)	Nose: 0.60		0.7	0.6		20
				Mouth: 0.80					
		Tang et al <sup>18</sup>	Propagation velocity (m/s)	Nose: 1.40		5	4.5		20
				Mouth: 1.30					
Tang et al <sup>18</sup>		Propagation area (m <sup>2</sup> )	Nose: 0.11		0.2	0.2		20	
			Mouth: 0.18						
	Area expansion rate (m <sup>2</sup> /s)		Nose only: 0.16	1.5	2				
	Mouth only: 0.17								
Tang et al <sup>18</sup>	Propagation distance (m)			F: 0.16-0.55			20		
				M: 0.31-0.64					
				F: 2.20-5.00					
				M: 3.20-14.00					
Tang et al <sup>18</sup>	Propagation area (m <sup>2</sup> )			F: 0.01-0.11			20		
				M: 0.04-0.14					
				F: 0.15-0.55					
				M: 0.25-1.40					
Schlieren PIV' velocimetry	Tang et al <sup>18</sup>	Maximum air speed (m/s)		8.00			16		
Particle image velocimetry	Savory et al <sup>28</sup>	Average of the spatially averaged maximum velocity after 1 m from mouth (m/s)		0.41			12		
	Kwon et al <sup>19</sup>	Average initial velocity (m/s)			M: 15.30		M: 4.07	26	
					F: 10.60		F: 2.31		
VanSciver et al <sup>25</sup>	Maximum velocity range (m/s)			1.15-28.8			29		
		Average max. velocity (m/s)		10.2 ± 6.7					
		Location of max. velocity (mm)		67.8 ± 78					

TABLE 1 (Continued)

Measurement techniques	Article	Main findings					No. of subjects
		Measured parameters	Breathing	Coughing	Sneezing	Speaking	
		Median velocity (m/s)		8.1			
		Jet width at 50 mm from mouth (mm)		35.8 ± 27.9			
	Chao et al <sup>27</sup>	Maximum air velocity (m/s)		M: 13.2 F: 10.2		M: 4.6 F: 3.6	11
		Average initial air velocity (m/s)		10.2		3.9	
	Zhu et al <sup>26</sup>	Initial velocity (m/s)		11.2			3
Pointwise measurement	Xu et al <sup>16</sup>	Thermal plume (m/s)	0.23				18
		Velocity at 3 mm from nose in standing position (m/s)	F: 1.63 M: 1.08				
		Velocity at 3 mm from nose in Lying position (m/s)	F: 1.52 M: 1.82				
		Centerline velocity (m/s)	Decay of centerline see Equation 1				
		Exhaled air temperature (°C)	36-32				
	Xu et al <sup>34</sup>	Relative humidity	80%				22
		Mean peak velocity at 3 mm from mouth (m/s)	F: 1.03 ± 0.51 M: 0.81 ± 0.4				
		Propagation distance (m)	0.3				
		Turbulence intensity at 3 mm from mouth	41 ± 5%				
	Gupta et al <sup>15</sup>	Change of airflow rate over time (L/s)	Sine function			1.6	25
	Gupta et al <sup>14</sup>	Change of airflow rate over time (L/s)		Combination of gamma probability distribution functions			25

Abbreviations: F, female; M, male.

namely the propagation distance and the propagation velocity. The propagation distance is defined as the distance between the mouth/nose of the subject and the tip of the exhaled jet as shown. The propagation velocity corresponds to the speed at which the jet tip travels.

### 2.1.1 | High-speed photography

The high-speed photography is used for flow visualization and provides information regarding the flow shape and its propagation such

as the flow direction, spread angle, and propagation velocity. To visualize the airflow, a high-speed camera is used to capture the motion of tracer particles like cigarette smoke or theatrical fog. The used tracer particles are fine enough to closely follow the airflow.

This technique was applied by Gupta et al<sup>14</sup> to identify the boundary conditions of the airflow exhaled during coughing, breathing, and speaking.<sup>15</sup> In this study, cigarette smoke was used as a tracer assuming that the 0.2  $\mu\text{m}$  smoke particles closely follow the airflow.<sup>14</sup> In order to visualize the airflow, five smoking subjects were photographed using a black background and a light source beneath the subject's face. This technique provides images with visible smoke particle concentration gradient which allows a rough estimation of both airflow direction and spread angle. As shown in Figure 1, the flow direction is defined as the angle between the flow center and the horizontal. Such angles can be determined by analyzing the side view photography. Table 2 compares the angle values obtained by Gupta<sup>14,15</sup> with other studies from literature.<sup>16-19</sup>

Likewise, front view photography of the subjects was used to determine the mouth and nose opening areas. The latter information

is important to provide boundary condition for flow modeling. Gupta et al photographed the subject's nose and mouth during coughing,<sup>14</sup> speaking,<sup>15</sup> and breathing.<sup>15</sup> The values of these areas are shown in Table 1, though a noticeable difference in nose and mouth opening area has been found between subjects.

Bourouiba et al<sup>20</sup> used the high-speed imaging technique to analyze sneezing and coughing. The authors used exhaled droplets of small diameters as a tracer. Whenever the concentration of droplets was too low, the visualizations were enhanced with a smoke generator. The visualizations showed that the cough lasts 300 ms while the sneeze duration is shorter (200 ms). Both coughing and sneezing exhaled jets were considered as turbulent since the Reynolds number for coughing and sneezing were 10 000 and 40 000, respectively. Bourouiba et al analyzed the flow shape in the first 70 cm from the mouth, and they noticed a change in the flow direction at the middle of this distance. As illustrated in Figure 1, the first part of the flow near the mouth (prior to the change of flow direction) was referred as the jet phase by Bourouiba et al, while the subsequent phase was referred as the puff phase. The authors defined the entrainment

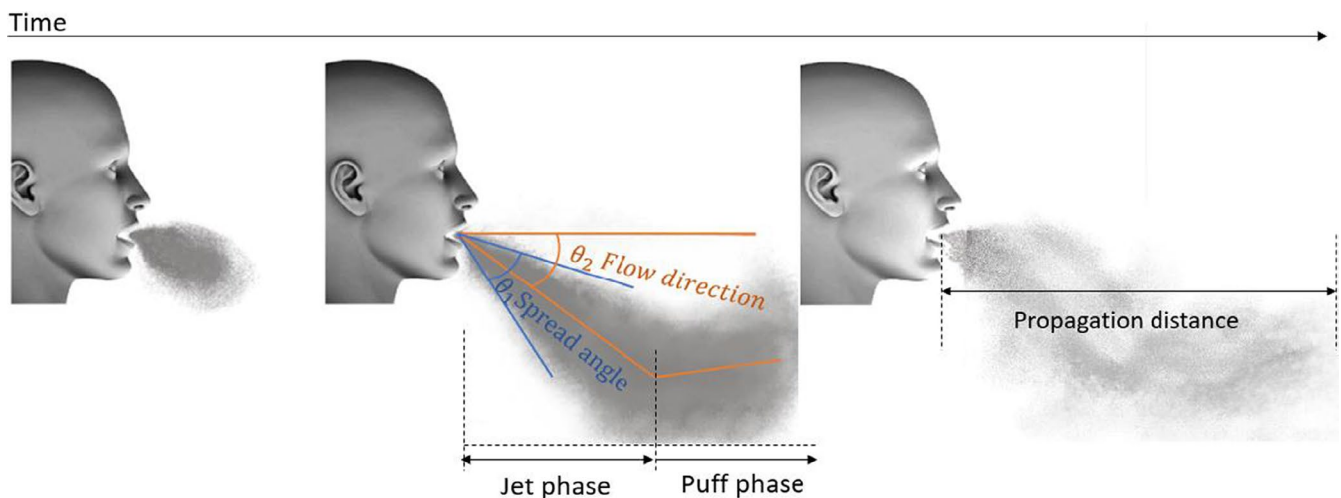


FIGURE 1 The flow direction and flow spread angle

TABLE 2 The direction and the spread angle of the exhalation jet from the literature

Exhalation mode	Source	Flow direction		Spread angle	
		Mouth	Nose	Mouth	Nose
Breathing	Xu et al <sup>16</sup>	14° ± 14°	57° ± 6°	36° ± 6°	32° ± 3°
	Tang et al <sup>17</sup>	Horizontal	45°-30°	-	-
	Gupta et al <sup>15</sup>	Horizontal	60° ± 6°	30°	23° ± 14°
Coughing	Bourouiba et al <sup>20</sup>	-	-	27°	-
	Kwon et al <sup>19</sup>	-	-	36°	-
	Tang et al <sup>18</sup>	-	-	23.9° ± 3.4°	-
	Gupta et al <sup>14</sup>	27.5° ± 5.9°	-	25° ± 6.4°	-
Speaking	Kwon et al <sup>19</sup>	-	-	59°	-
	Gupta et al <sup>15</sup>	-	-	30°	-
Sneezing	Bourouiba et al <sup>20</sup>	-	-	14.8°	-

coefficient  $\alpha$  as the slope of the linear relation between the jet radius and the travel distance from the mouth. With this definition, the relation between  $\alpha$  and the spread angle  $\theta_1$  is  $\alpha = \tan(\theta_1/2)$ . As for coughing, Bourouiba et al reported an entrainment coefficient of 0.24 in the jet phase which corresponds to a spread angle of 27°. This value matches well with those obtained by Tang et al<sup>18</sup> and Gupta et al<sup>14</sup> as shown in Table 2. Thanks to the high-speed photography technique, the authors identified the value of the puff phase entrainment coefficient, which is almost half of the jet phase one, corresponding to a spread angle of 15°. Likewise, a similar decomposition of the flow into a jet phase and a puff phase was also made for the sneezing activity. The entrainment coefficients values were 0.13 and 0.055 for the jet and puff phases, respectively, which corresponds to spread angles of 14.8° and 6.3°.

The high-speed photography technique was not only applied on human subjects. Liu and Novoselac<sup>21</sup> built a cough box or cough generator with a volume of 15.6 L. Air was injected inside this box with a square wave temporal profile, and with a time step of 1 second. The airflow was visualized by using a fog machine that generates particles with diameters lower than 2.5  $\mu\text{m}$  in size. The analysis of the flow shape revealed that the jet propagates more than 0.2 m in 0.1 second. The observation of the flow boundaries allowed the determination of the spread rate, which is defined as the ratio between the radial expansion of the jet and the horizontal propagation. The captured images showed the creation of a circular vortex, also known as the leading tip, in the front of the jet during the first 0.15 second.

### 2.1.2 | The schlieren photography

The schlieren photography technique is based on the variation of the air refractive index with the density. In the case of human exhalation flows, a density gradient is induced by the temperature difference between the ambient air and the exhaled air. Although the exhaled air temperature varies with the climatic conditions, it is usually higher than the ambient air. In laboratory conditions with 50% relative humidity and 20°C, the air is exhaled from the nose at a temperature value close to 34°C.<sup>22</sup> The schlieren technique can be used to study the flow shape and analyze its propagation in the surrounding environment. Tang et al implemented this technique to observe the breathing,<sup>17</sup> sneezing,<sup>17</sup> and coughing<sup>23</sup> of 20 healthy volunteers (10 females and 10 males). They used a high-speed camera to capture images of exhalation that were later automatically processed. The automation of the image processing allowed the authors to analyze a large number of images and to extract data about the visible projected area and the propagation distance at a high frequency. Tang et al<sup>23</sup> reported that the average horizontal propagation distance of coughing was in the range of 0.16–0.64 m however, when they reprocessed the images in another study<sup>17</sup> considering the propagation on the main flow direction they found that the maximum distance is 0.7 m and the maximum derived velocity is 5 m/s. Pepper sneeze stimulus was used to help six volunteers to sneeze and the

sneeze puff travelled 0.6 m with a propagation velocity of 4.5 m/s.<sup>17</sup> By analyzing the schlieren imaging for nasal and mouth breathing, they found that the air travels 0.6 m with a velocity of 1.4 m/s in the case of nasal breathing, while it propagates more slowly at a velocity of 1.3 m/s over longer distance—0.8 m—in the case of mouth breathing.<sup>17</sup> When analyzing these data, it is important to keep in mind that these distances are characterized by the temperature/density gradient and not the local airflow velocity. Further results of the breathing flow shape and direction obtained by<sup>17</sup> are presented in Table 2.

Another study by Xu et al<sup>16</sup> used schlieren photography technique to visualize the breathing airflow in standing and lying positions of 18 healthy subjects at 23°C room temperature. They noticed that the flow shape, direction, and propagation seem to vary from one person to another. However, they were able to determine average values of the jet direction and spread angle for mouth only and nose only breathing which are reported in Table 2. Images recorded by the high-speed camera demonstrated that the ring vortices flow structures at the jet boundary of built by successive breathing cycles are connected, having similar characteristics to these observed in a steady turbulent jet. In addition to this qualitative result, the schlieren analysis allows to investigate the interaction between the body thermal plumes and the exhalation flow. With this technique, two main effects of this interaction were noticed: In the standing position, the raising body thermal plume interacts with the exhaled air drifting it upwards while for the laying position the direction of the thermal plume is the same as the exhaled flow therefore enhancing the upward air movement.

### 2.1.3 | Particle image velocimetry

The Particle Image Velocimetry (PIV) technique has been widely used in the field of indoor air because it provides essential detailed quantitative information on the flow fields.<sup>24</sup> In this PIV technique, a pulsed laser light sheet illuminates the tracer particles in a measurement plane, and a synchronized CCD camera acquires two single exposed images taken shortly one after another. By comparing these two pictures, the travelled distance of individual particles can be determined, and it corresponds to the displacement field of tracer particles. The velocity field is then calculated by dividing the displacement field by the time step of a few microseconds order. The PIV has been used to characterize the airflow field formed by coughing<sup>19,25–27</sup> and speaking.<sup>19,27</sup> In these studies, the subjects were asked to cough into a chamber which was filled with submicronic particles of titanium dioxide,<sup>28</sup> olive oil,<sup>19</sup> saline fog,<sup>27</sup> or glycols solutions.<sup>25</sup> The motion of the tracer particles is recorded a few microseconds after the beginning of the exhalation event with a typical time step of 100  $\mu\text{s}$ . Thus, the PIV can provide a quantitative measurement of the velocity flow field for highly unsteady flows like coughing and speaking. However, there are two main limitations for this technique. First, the health hazards arise from using the tracer particles and the laser when conducting the experiments on human subjects impose technical constraints. Second, the exploration area is

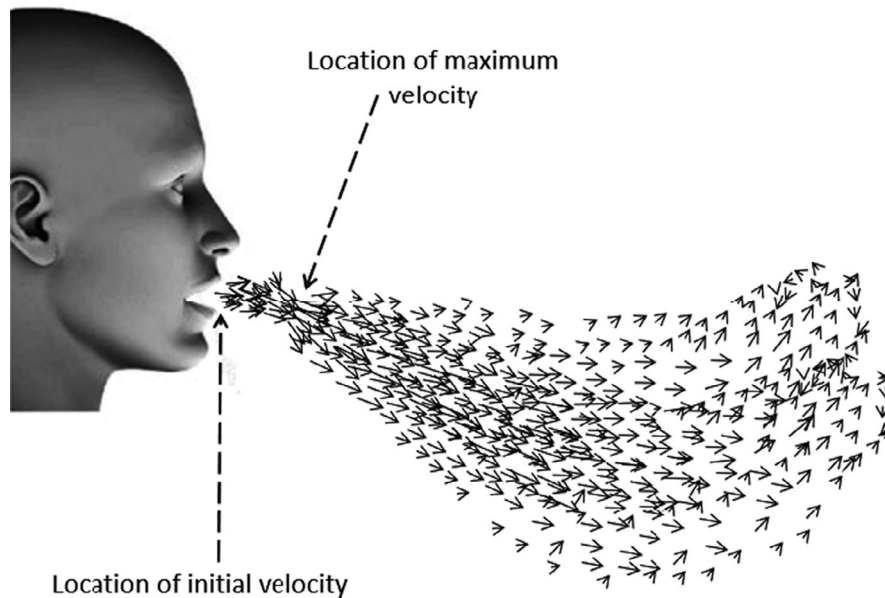


FIGURE 2 Schematic figure for the velocity flow field during exhalation

limited, a typical optical configuration of the PIV as in Savory et al<sup>28</sup> forms a measurement area of 400 cm<sup>2</sup>.

VanSciver et al.<sup>25</sup> asked 10 males and 19 females to cough into a 120 cm × 76 cm × 67 cm chamber to analyze the airflow field and the maximum coughing velocity. They recorded a wide range for this maximum velocity; from 1.15 to 28.8 m/s while the average maximum velocity was 10.2 m/s. The authors found that the maximum velocity of the airflow usually happens at a distance of 3.9–309 mm from the mouth because of the vena contracta phenomenon. The vena contracta phenomenon happens with the sudden change of the cross-sectional area of the flow geometrical boundaries. As the exhaled flow direction cannot be quickly adjusted to the sudden increase of the flow area after the mouth, it continues to contract, and the minimum flow area corresponding to the maximum air speed occurs after the mouth as illustrated in Figure 2.

This maximum velocity is reached 20  $\mu$ s after the beginning of the cough. Then, it decreases by 74% after 0.67 second. Through the postprocessing of the velocity field obtained by PIV technique, it is possible to build velocity profiles at different locations in the jet to analyze its expansion. VanSciver et al defined the width of the jet by considering the upper and lower locations where the velocity is half of the maximum profile velocity. They reported a linear jet expansion over the first 200 mm from the mouth. The Reynolds number for coughing exhaled jet was in the range of 2300–57 600 and the average Reynolds number was 20 400, which is in accordance with the value of 10 000 obtained by Bourouiba et al<sup>20</sup> for a single subject.

Considering these values of the velocity and the size of the box, the authors suspected that the results could be affected by the confinement effect due to the small size of the box (1.2 m in length). However, in another study,<sup>26</sup> three subjects coughed in a chamber of 180 cm × 180 cm × 180 cm and the average maximum velocity was 11.2 m/s, only 10% higher than the value reported by VanSciver et al. This slight difference could be attributed to the individual

differences between subjects and it does not confirm the effect of the confinement. In the study of Zhu et al,<sup>26</sup> the range of the maximum velocity was between 6 and 22 m/s. However, values greater than 18 m/s were very rarely observed. Savory et al<sup>28</sup> used PIV to investigate the velocity at 1-m distance from the mouth for 12 healthy individuals. They assumed that studying the far field velocity would be of particular interest for disease transmission studies. This study reveals that at 1-m distance the cough affects the air velocity field and the measured average velocity value is 0.41 m/s.

Kwon et al<sup>19</sup> and Chao et al<sup>27</sup> used the PIV technique to analyze the velocity field near the mouth produced by coughing and speaking. They defined the *initial velocity* as the highest velocity measured during the coughing process. The initial velocity distribution diagram built from measurements with a 26 volunteers group by Kwon et al showed that this initial velocity of the cough lies within a 6–13 m/s range, with an average initial coughing velocity of 15.3 m/s for males and 10.6 m/s for females. The results of Chao et al were in accordance with the other studies discussed in this section: The authors reported an average coughing velocity of 11.7 m/s. Although it is challenging to characterize airflows produced during speaking activity (because of its dependence on the pronounced sounds), Kwon et al and Chao et al obtained comparable results. The protocol for Kwon et al experiment consisted in counting from one to three in Korean while it was counting from 1 to 100 ten times in Chao et al study. The average maximum measured speaking velocity by Kwon et al was 4.07 m/s for males and 2.31 m/s for females, and for Chao et al, it was 3.9 m/s. Chao et al also mentioned that the propagation distance for coughing was higher than for speaking and that the entrainment of the ambient air was noticeable in both cases. Further vector analysis was conducted by Kwon et al to identify the jet spread angles and the values obtained are compared with the other values in the literature<sup>14,15,18</sup> in Table 2.

As discussed above, health hazards arise when using the PIV technique on human subjects; it requires to apply safety procedures, in particular those to make sure that the tracer particles are confined in the measurement chamber. This makes the study of the airflow near the subject's body difficult. Moreover, it eliminates the effect of the body thermal plume on the exhaled airflow. To overcome these constraints, researchers developed thermal breathing manikins to simulate the human exhalation activities and enhance the study of the airflow in the human microenvironment. Feng et al<sup>29</sup> used a thermal breathing manikin together with a two-dimensional time-resolved particle image velocimetry system, to obtain detailed data on averaged flow fields, vorticity, and turbulence intensity, for further comparison with CFD simulations. The manikin was breathing in horizontal direction through a mouth opening of 12 mm diameter. The airflow rate was 0.45 L per exhalation following a sinusoidal pattern with a frequency of 15 breaths per minute. In order to study the thermal plume, the exhaled air temperature was kept in the range of 32–36°C, and the body of the manikin was heated using a 75 W heater. Feng et al applied the phase-averaged method to analyze the results of the PIV. They divided the breathing process into 40 phases, 20 for exhalation and 20 for inhalation, and the velocity values were averaged over each phase. This study showed that during the middle phases, the flow shape and the linear spread of the airflow were similar to those of the free jet. The use of the PIV permitted to identify the formation of two large vortices on the two sides of the jet in the initial stage. These vortices evolve and are more noticeable during the middle phases when higher turbulence intensity is measured. The use of the thermal breathing manikin and the phase average approach produced statistically acceptable data to study the flow turbulence. The maximum turbulence intensities were measured near the centerline of the flow where the exhaled flow interacts with the thermal plume that drifts the jet flow upward.

With the same manikin as Feng et al, Jiang et al<sup>30</sup> studied the characteristics of the exhaled air parameters during breathing. The effect of the thermal plume was analyzed by building the contour map for the normal velocity. Jiang et al used the proper orthogonal decomposing to divide the flow into four different parts: main-flow part, coherent part, transient, and turbulent part. The main flow contains most of the flow energy, and the fluctuations are divided between the other three parts. The authors noticed that during the late phases of exhalation the thermal plume contributed in enlarging the coherent part of the flow which means that the thermal plume enhances the flow turbulence.

Another study by Berlanga et al<sup>31</sup> used PIV and the phase average approach to study and analyze the velocity field of the human exhalation of an average male (test M) and an average female (test F), using a life-sized thermal manikin. They used CO<sub>2</sub> as a tracer, and with the help of a high-resolution camera, they studied the flow direction and propagation. The manikin was in lying position and so the flow had a vertical direction and the exhalation had sinusoidal pattern with a flow rate of 9.45 L/min for

(test M) and 7.52 L/min (test F). The comparison of results for the (test M) and (test F) showed that although the flow shape is almost the same, the propagation distance for the (test M) was higher than (test F) and the diffusion angle was wider, 20.5° for (test M) and 22.7° for (test F).

## 2.2 | Pointwise measurements

Here, pointwise measurements refer to quantitative measurements performed by using probes at a given point in the flow field. This includes measurements for velocity, temperature, humidity, and airflow rate. The pointwise measurements provide accurate quantitative information. However, those measurements require a lot of time and effort to obtain a full picture of the flow. To overcome this difficulty, the pointwise measurements techniques are often preceded by one kind of global flow-field techniques.

As shown on Table 1, coughing is by far the most-studied exhalation mode because of its important impact on disease transmission. Preliminary studies<sup>32,33</sup> aimed to examine the coughing flow rate, which is usually characterized by three following parameters; Cough Peak Flow Rate (CPFR), Cough Expired Volume (CEV) which is the total volume expired during the cough, and Peak Velocity Time (PVT) which is the time between the beginning of the cough and the time at which the maximum velocity occur. Using regression analysis, relationships between these parameters and the height, weight, gender, and age of the person were proposed by Mahajan et al<sup>32</sup> and Singh et al<sup>33</sup>. Gupta et al<sup>14,15</sup> measured the airflow rate of 25 healthy subjects for coughing, breathing, and speaking using a spirometer. They found that the cough airflow rate can be described using a combination of gamma probability distribution functions while the normal breathing airflow rate follows a sine function over time and this function depends on the subject height and weight.<sup>15</sup> The value obtained for the duration of a single cough was in the range of 0.26–0.78 second, which is in accordance with the value obtained by means of high-speed photography of 0.3 second by Bourouiba et al.<sup>20</sup> The airflow rate during speaking might be the most difficult to measure as it depends on the pronounced sounds. To characterize the airflow rate for speaking, Gupta et al<sup>15</sup> used a spirometer to measure the exhaled airflow during three exercises: counting from 1 to ten, pronouncing six letters and reading a passage. Pronouncing T letter resulted in 2 L/s flow rate and it was the highest expelled flow rate. Consequently, pronouncing number two and ten produced more airflow. The peak flow rate measured during passage reading was 1.6 L/s.

In addition to the airflow measurements, Xu et al<sup>16</sup> conducted velocity pointwise measurements for the breathing airflow. For optimized experimental planning, these measurements were preceded by schlieren photography in order to estimate the centerline of the airflow. Using a hot sphere anemometer, pointwise measurements for velocity were taken along the flow centerline at different distances from the mouth/nose. The average *initial breathing velocity* was measured at 0.03 m from nose. In the standing position, the



measured initial velocity was 1.08 and 1.63 m/s for male and female, respectively. According to Xu et al, the decay of the centerline velocity could be expressed by the following power function:

$$U_m = ax^b \quad (1)$$

where  $U_m$  is the centerline velocity and  $x$  is the distance from the mouth/nose.  $a$  and  $b$  are constants which depend on gender and mode of breathing (mouth or nose).

As discussed above, manikins can be used to overcome technical constraints but there are differences between human and manikin exhalation. To evaluate these differences, Xu et al<sup>34</sup> compared the characteristics of breathing from a human subject and a thermal breathing manikin using hot sphere anemometer. The manikin had two 12-mm-diameter circular openings (nose openings) and a semi-elliptical mouth of 120 mm<sup>2</sup>. Sinusoidal breathing was modeled with a frequency of 15.5 breaths per min and a respiratory minute volume of 8.8 L/min. This respiratory minute volume is the amount of air exhaled or inhaled during one minute. The measured temperature of the exhaled air was 34°C while the room temperature was kept at 20°C. Xu et al noticed that the sinusoidal breathing of the manikin produces the same velocity profile as the human subject but with different respiratory frequency and magnitude. These differences result in a significant underestimation of the turbulence levels as the turbulence intensity on the center line was (41 ± 5) % for the subject and 1.3% for the manikin. The velocity profile was obtained by measuring the velocity of the air in different vertical planes at given distances from the source. The airflow from the manikin was similar to the turbulent circular jet and the propagation distance was around 0.3 m for the subject and 0.4 m for the manikin. The authors compared those results with the results of the previous studies<sup>17,23</sup> obtained by applying the schlieren photography technique, and they suggested that using the schlieren technique might overestimate the propagation distance of the flow. This overestimation might be attributed to temperature diffusion rather than the travel of the gas.

Another study by Xu et al<sup>35</sup> also used pointwise measurements to investigate the effect of the ventilation and the metabolic rate on the dispersion of exhaled droplets. The metabolic rate corresponds to the amount of consumed energy by the body per unit of time. The metabolic equivalent of task (met) corresponds to a reference metabolic rate of 1.163 W/kg, which is roughly equivalent to the amount of energy expended at a sitting position. To study the effect of body activity, the thermal breathing had two metabolic rates, 1.2 met and 2 met. The measurements were conducted in a room with two ventilation methods, room mixing ventilation and displacement ventilation, to compare between them. Xu et al<sup>35</sup> reported that the velocity profiles of the sinusoidal exhaled airflow were similar to those of the steady jet. Based on results obtained by the high-speed photography technique, Liu and Novoselac<sup>21</sup> conducted quantitative measurements of the jet flow centerline velocity using a hot wire anemometer and a hot sphere anemometer at 76 positions. Table 3 summarizes the characteristics of the manikins used in the previous studies and measured parameter.

### 3 | MEASUREMENTS ON THE EXHALED DROPLETS

As discussed in the introduction, the exhaled air jet carries droplets with a polydispersed size distribution. Studies on the characterization of the exhaled droplets mainly focus on determining the size of the initial droplets as it is the main parameter governing their fate, either they deposit on a surface or remain suspended and carried by the airflow.<sup>36</sup> The size of the droplets is also associated with their composition and the likelihood of bearing pathogens. A study by Milton et al<sup>37</sup> examined particles exhaled from 37 seasonal influenza-infected patients. The study showed that fine particles—smaller than 5 µm—contain 8.8 fold more viral copies than coarse particles—bigger than 5 µm. Similarly, Lindsey et al<sup>38</sup> found that 42% of influenza RNA is detected in particles smaller than 1 µm, while 23% is in particles of 1 to 4 µm, and 35% in coarse particles bigger than 4 µm. Fabian et al<sup>39</sup> conducted another observational study on 12 laboratory-confirmed influenza patients. In this study, they observed that during tidal breathing, 87% of the particles sampled from patients' exhalations were <1 µm. After detecting the presence of RNA in part of these fine particles, Fabian et al concluded that sub-micronic aerosols could have an important contribution to the influenza transmission process. These different results can be linked to the relation between the droplet size and its origin in the respiratory tract. Morawska et al<sup>11</sup> analyzed the modes of particles produced by different exhalation activities. They found that normal breathing produces particles of 0.85 µm mode, the vocal cord vibration mode is 3 µm, and oral or saliva mode is 10 µm.

After their release, the droplets go through a very rapid evaporation process and transform to dry residues which are mainly composed of NaCl and organic component.<sup>40</sup> Figure 3 illustrates both the change of the size distribution of the exhaled droplets at different distances from the mouth and the settling drift of large diameter droplets due to gravity. When choosing a measurement technique, it is critical to look at the place of the measured droplets with respect to this evaporation process. Some measurement techniques involve sampling and travel of the droplets from the sampling point to the measurement location. During this travel, evaporation might occur which induces a change in the measured droplet size. So, these techniques are well adapted to measure the size of dry residues after the complete evaporation of the droplets, but they can be also used to predict the initial droplet size distribution by applying some calibration process or evaporation model. In our review, all the techniques involving the extraction/collection of a sampled airflow with particles are named *intrusive* techniques. *Non-intrusive* measurements are directly conducted in the flow stream without sampling.

Gralton et al.<sup>41</sup> reviewed the measured size of the exhaled particles in literature, including both droplets and dry residues, and they concluded that the exhaled particles have a size range between 0.01 and 500 µm. This size range can hardly be covered by a single measurement technique, which justifies the use of two kinds of techniques in most of the reviewed studies. Table 4 classifies the studies aimed at characterizing the respiratory droplets according

TABLE 3 The characteristics of the artificially produced jets and the measured parameters

Measurement technique	Manikin properties			Generated jet			Main studied parameters			
	Article	Exhalation mode	Opening area	Thermal load	Body thermal temperature (°C)	Continuity or frequency		Flow rate or velocity	Flow shape	Temperature °C
Visualization	Liu and Novoselac <sup>21</sup>	Coughing	Circular tube of 2.4 cm inner diameter	45 W		1 times/s	*initial velocity = 6.08 m/s	Square wave		<ul style="list-style-type: none"> <li>• Propagation distance</li> <li>• Spreading rate</li> </ul>
Pointwise anemometry										Comparison between steady jet and cough jet in terms of
	Xu et al <sup>35</sup>	Breathing	Mouth: 120 mm <sup>2</sup> (semi ellipsoid) Nose: 2 tubes, 12 mm diameter	70 W·m <sup>2</sup>		15.5 times/min	8.8 L/min		34	<ul style="list-style-type: none"> <li>• Centerline velocity</li> <li>• Velocity profile</li> </ul> Effect of body metabolic rate and ventilation on velocity profile
	Xu et al <sup>34</sup>	Breathing	Mouth: 120 mm <sup>2</sup> (semi ellipsoid) Nose: 2 tubes, 12 mm diameter	70 W·m <sup>2</sup>		15.5 times/min	8.8 L/min		34	<ul style="list-style-type: none"> <li>• Centerline velocity</li> </ul> Comparison between human and manikin breathing in terms of:
	Feng et al <sup>29</sup>	Breathing	12 mm diameter	75 W	32-36	15 times/min	0.45 L/exhalation time		34	<ul style="list-style-type: none"> <li>• Velocity field</li> <li>• Flow shape</li> <li>• Vorticity</li> <li>• Centerline Velocity</li> <li>• Turbulence intensity</li> </ul>
	Berlangaet al. <sup>31</sup>	Breathing	Mouth: 122 mm <sup>2</sup> (circular)	128 W	34	16.43 & 13.7 times/min	9.46 & 7.52 L/min		34	<ul style="list-style-type: none"> <li>• Velocity field</li> <li>• Flow shape</li> <li>• Jet spread angle</li> <li>• vorticity</li> <li>• Centerline Velocity</li> </ul>
	Jiang et al <sup>30</sup>	Breathing	Nose: 12 mm diameter	75 W		15 times/min	0.45 L/time	Sinusoidal	34	<ul style="list-style-type: none"> <li>• Velocity field</li> <li>• Spatial distribution of the turbulence intensity</li> <li>• Effect of the body thermal plume.</li> </ul>

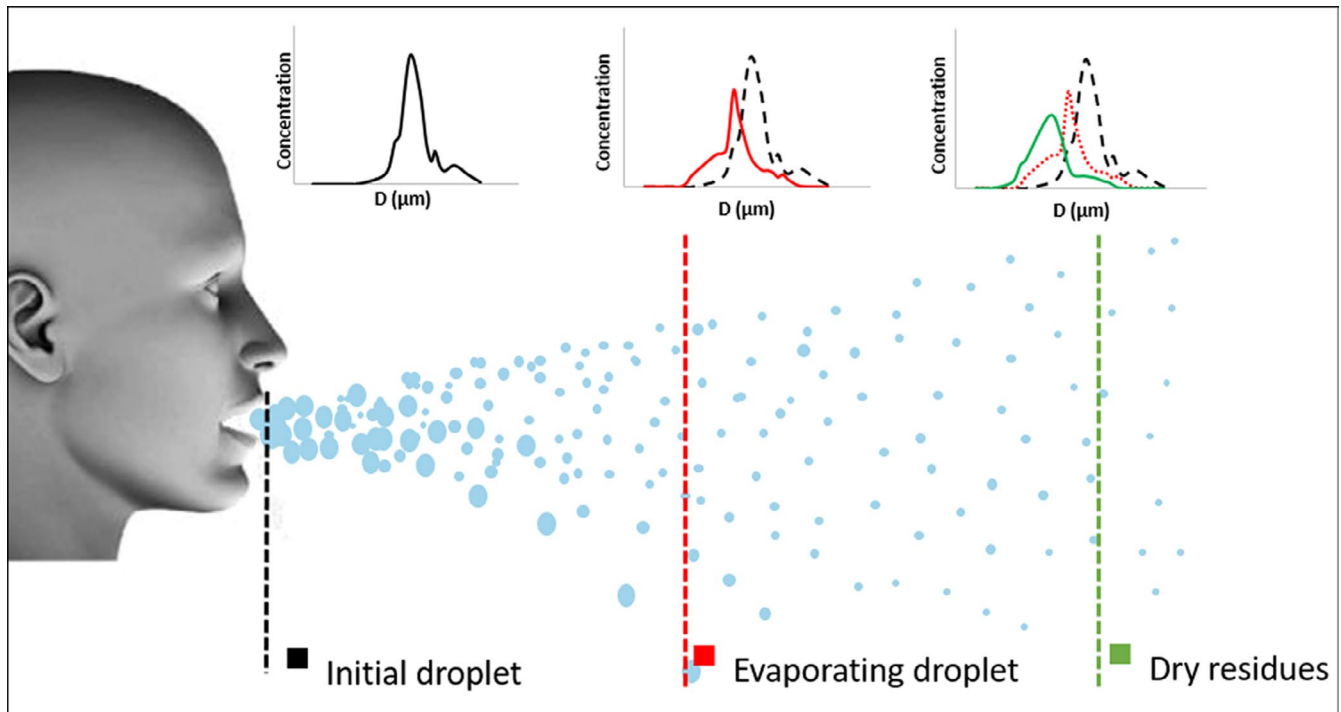


FIGURE 3 The change of exhaled droplets size distribution with distance

to the adopted measurements technique. The term *equivalent diameter* which appears in Table 4 is an important point when considering any aerosol size measurement technique. As each measurement technique is based on a specific physical property, the equivalent diameter is “the diameter of a sphere having the same value of a specific physical property”.<sup>42</sup> For example, the Aerodynamic Particle Sizer (APS) measures the particle aerodynamic equivalent diameter which is defined as the diameter of a sphere having a density of  $1000 \text{ kg/m}^3$  and the same gravitational settling velocity as the measured particle. The optical diameter corresponds to the diameter of the spherical particle scattering the same light amount as the analyzed particle. Baron et al<sup>42</sup> define the mobility equivalent diameter as “the diameter of a sphere with the same mobility as the particle in question”. Meanwhile, the geometric diameter is the diameter of the spherical particle which is usually obtained through direct measurement of the particle using a microscope or through a geometric analysis of the particle's image. Thus, the equivalent diameter should be considered when applying different measurement techniques or comparing their results.

### 3.1 | Intrusive measurement techniques

Solid impaction, droplet deposition, optical particle counter, and aerodynamic particle sizer are widely used intrusive measurements techniques. Solid impaction and droplet deposition were the techniques applied by the early studies, and then optical particle counter

and aerodynamic particle sizer were later used. Other techniques like Liquid impingers, Scanning Mobility Particle Sizer (SMPS), Electrical Low-Pressure Impactor (ELPI), and Condensation Particle Counter (CPC) are less cited in the existing literature and they are also discussed in the last subsection.

#### 3.1.1 | Solid impaction

Early studies used solid impaction technique to quantify the size distribution of the droplets expelled during coughing, sneezing, breathing, and speaking. In addition to the size information, collected droplets can be used for further biological tests. Duguid<sup>43</sup> studied the size distribution of the initial droplets produced during speaking, sneezing, and coughing using impaction plates placed in front of the subjects' mouth, at 3 and 6 inches, respectively, in the cases of speaking and coughing/sneezing. For a better visualization of the droplets, Duguid applied dye on the surfaces of the mouth and fauces. To calculate the diameter of the initial droplets, a calibration procedure was applied to find the relationship between the size of the stain marks remained on the celluloid-surface of the impaction plate and diameter of the initial droplets. The size of the initial droplets was in the range of  $5\text{--}2000 \mu\text{m}$ , and it is assumed that droplets with a diameter lower than  $5 \mu\text{m}$  might evaporate quickly or be driven by the deflected flow around the impaction plate. Duguid also used another solid impaction device which is the slit sampler also known as slit impactor to collect the suspended dry residues from

TABLE 4 The techniques used for the characterization of the respiratory droplets

Technique	Measured parameters	Size range	Equivalent diameter	Articles
<b>Intrusive</b>				
Solid impaction	<ul style="list-style-type: none"> <li>• Size distribution of dry residues and initial droplet</li> <li>• Concentration of pathogens in the exhaled air</li> </ul>	–	Aerodynamic diameter	Duguid, <sup>43</sup> Milton et al, <sup>37</sup> Fennelly et al <sup>44</sup>
Droplet deposition analysis	<ul style="list-style-type: none"> <li>• Size distribution of initial droplet</li> <li>• Concentration of initial droplet</li> </ul>	–	Geometric diameter	Duguid, <sup>43</sup> Loudon and Roberts, <sup>45</sup> Li et al, <sup>46</sup> Xie et al <sup>47</sup> Morawska et al <sup>57</sup>
Optical particle counter	<ul style="list-style-type: none"> <li>• Size distribution of dry residues and initial droplet</li> <li>• Concentration</li> </ul>	0.3-20 $\mu\text{m}$	Optical diameter	Fabian et al <sup>39</sup> Fabian et al <sup>49</sup> Edwards et al, <sup>50</sup> Holmgren, <sup>50</sup> Almstrand et al, <sup>52</sup> Papineni and Rosenthal <sup>53</sup> Li et al <sup>46</sup> Xie et al, <sup>47</sup> Wurie et. al, <sup>54</sup> Wurie et. al. <sup>55</sup>
Aerodynamic particle sizer	<ul style="list-style-type: none"> <li>• Size distribution of dry residues or evaporating droplets</li> <li>• Concentration</li> </ul>	0.5-20 $\mu\text{m}$	Aerodynamic diameter	Yang et al <sup>63</sup> Morawska et al <sup>57</sup> Liu Novoselac <sup>21</sup> Fang et al <sup>58</sup> and Asadi et al <sup>59</sup>
The electrical low-pressure impactor	<ul style="list-style-type: none"> <li>• Size distribution of dry residues</li> </ul>	0.007-10 $\mu\text{m}$	Aerodynamic diameter	Hersen et al <sup>62</sup>
The Scanning Mobility Particle Sizer	<ul style="list-style-type: none"> <li>• Size distribution of dry residues</li> <li>• Concentration</li> </ul>	0.02-0.6 $\mu\text{m}$	Mobility diameter	Yang et al <sup>63</sup>
Filter collection	<ul style="list-style-type: none"> <li>• Size distribution of dry residues</li> </ul>		Geometric diameter	Loudon and Roberts <sup>45</sup>
<b>Non-intrusive</b>				
High-speed photography	<ul style="list-style-type: none"> <li>• Particle dynamics and propagation</li> </ul>	It depends on the laser and optical configuration of the system	–	Zhu et al, <sup>26</sup> Nishimura et al, <sup>64</sup> Bourouiba et al <sup>20</sup>
Laser particle size analyzer	<ul style="list-style-type: none"> <li>• Size of evaporating droplet</li> <li>• Concentration</li> </ul>	0.1-1000 $\mu\text{m}$	Optical diameter	Han et al, <sup>67</sup> Zayas et al <sup>68</sup>
Interferometric Mie Imaging	<ul style="list-style-type: none"> <li>• Size distribution of droplet</li> <li>• Concentration</li> </ul>	>2 $\mu\text{m}$	Optical diameter	Chao et al, <sup>27</sup> Chao and Wan <sup>66</sup>

the air on a rotating agar plate. On this plate, pathogens contained in the dry residues multiply in the agar culture medium and form visible colonies that can be counted. By measuring the air volume extracted during sampling, Duguid determined the number concentration of the viable dry residues. The slit impactor was also used by Milton et al<sup>37</sup> to collect and analyze the influenza virus carried by droplets in the breath of infected individuals. They designed a conical hood into which the subject breathes to gather the exhaled air. Then, the captured air passes through a conventional 5  $\mu\text{m}$  cutoff diameter slit sampler to collect large droplets. A water vapor condensation process on the fine particles, less than 5  $\mu\text{m}$ , was then used to grow the size of these particles so that they could be collected with a 1  $\mu\text{m}$  cutoff diameter slit sampler. This procedure permits

the biological analysis of the fine fraction of exhaled droplets. A six-stage Andersen cascade impactor which is another solid impaction device was used by Fennelly et al<sup>44</sup> to study the concentration and size distribution of infectious aerosols exhaled by patients with tuberculosis. The Andersen impactor used by Fennelly and the slit impactor provide information about the number concentration of the viable pathogens but not the size of the droplets or the dry residues. Although the particles are classified into six size classes in the case of the Andersen impactor, the obtained size distribution cannot directly represent neither the size distribution of the initial droplets nor the dry residues because the evaporation process between the collection point close to the patient mouth and the impactor is not evaluated.

### 3.1.2 | Droplet deposition analysis

Droplet Deposition Analysis (DDA) is one of the techniques that has been used to determine the size distribution of the initial exhaled droplets. It requires building a correlation between the diameter of a droplet deposited on a surface forming a stain mark and the initial diameter of the droplet. Two types of droplets deposition experimental setups have been developed. The first setup was designed by Loudon and Roberts,<sup>45</sup> and it consists in a closed box with about 57 L capacity and the walls were covered by high grade white boned papers. One of the wall sides contains an inlet opening through which the subject exhales breaths into the box. In the experiment, the mouth of each subject was colored with a dye. After a given number of exhalations, the size and number of the stain marks on the floor, opposite, right, and left side of the box produced by the droplets' deposition were determined by microscopic observation. Li et al<sup>46</sup> designed a box with the same characteristics of the one of Loudon and Roberts. Water sensitive paper was used instead of the white boned paper. This paper type has a yellow coating that turns into blue color with water contact. This particular property of the paper makes it possible to analyze the droplet size and number without using dye. Xie et al<sup>47</sup> used the box designed by Li et al to measure the droplets size distribution produced during coughing and speaking. They evaluated the impact of using the dye on the measured droplet size distributions. The water sensitive paper used in Li et al experiment was replaced by glass slides in this experiment. The subjects exhaled in the box with and without using the dye and the size distribution of the droplets deposited on the glass slides was measured using a microscope. They concluded that the use of dye increases the production of droplets during human exhalation activities.

The second type of experimental setup is the one designed by Morawska et al,<sup>11</sup> which consists in a wind tunnel where the head of the subject can be inserted. The air circulating inside the tunnel is filtered with a High Efficiency Particulate Air (HEPA) filter which ensures that the only source of particles inside the tunnel is the subject itself. Glass slides were placed in several locations downstream of the subject head, on the floor of the tunnel, to collect deposited particles. Using the same experimental setup, Johnson et al<sup>48</sup> studied the modes of exhaled droplets size distribution with the objective of linking these modes to their sites of origin in the respiratory tract. The droplet of diameter  $<20\ \mu\text{m}$  was most likely remain airborne, so  $20\ \mu\text{m}$  was consider as the lower detection limit of this system. The exhaled airflow rate was also estimated to obtain the droplet number concentration.

### 3.1.3 | Optical particle counter

Optical Particle Counters (OPC) provide a determination of the optical equivalent diameter of the particle as a function of the light scattered by the particle when it crosses a light beam emitted by a white light or laser source. The air is extracted from the breathing zone of the subject through a mouthpiece which is a collection device that delivers the exhaled breath from the mouth of the subject to the

inlet of the OPC. The OPCs are used to measure size and number concentration of the particles in the size range  $0.3\text{--}20\ \mu\text{m}$  divided into 4,<sup>39,49</sup> 6,<sup>50</sup> or 15 size intervals.<sup>51</sup> One of the advantages of this extractive technique is that it permits conducting parallel measurements using other techniques such as impactors<sup>52</sup> or filters.<sup>49</sup>

Papineni and Rosenthal<sup>53</sup> compared Droplet Deposition Analysis (DDA) with Optical Particle Counter (OPC) direct measurements. They reported that the OPC is more practical and less time consuming when compared to the tedious process of measuring and counting the droplet by the microscope for DDA. However, they estimated 23 milliseconds traveling time of the particles from the sampling point to the measurement point. To evaluate the impact of this transfer on the droplet diameter, Papineni and Rosenthal carried out two experiments to evaluate the condensation and the evaporation. The experiments demonstrated that there is no formation of new droplets inside the OPC due to condensation, and that evaporation was not observed. A predominance of the particles of  $<1\ \mu\text{m}$  in diameter was noticed in the measurements obtained by the OPC while the particle concentration was more heavily weighted toward larger particles in the case of the DDA, even though dry residues were measured. The authors attributed this discrepancy to the instrumentation deficiencies in both techniques. On one hand, the low concentration of the small particles detected by the DDA system could be due to the large cutoff diameter caused by the small collection surface of the impactor used, or the limited resolution of the microscope. On the other hand, large droplets might be undetected by the OPC systems due to the sampling losses in the mouthpiece and the delivery lines. In another study,<sup>39</sup> the exhaled breath of 10 influenza infected patients was analyzed using OPC. The size and number concentration were measured, and the results were similar to those of Papineni and Rosenthal, as 87% of the detected particles have a diameter  $<1\ \mu\text{m}$ . The number concentration of the droplets in the size range of  $0.3\text{--}0.5\ \mu\text{m}$  was 61-3848 Particle/L and for the size range of  $0.5\text{--}1\ \mu\text{m}$  was 5-2756 Particle/L. The predominance of the submicronic particles for both healthy and rhinovirus (HRV)-infected subjects was noticed in a third study.<sup>49</sup>

Wurie et al<sup>54</sup> used the OPC to characterize the size distribution and concentration of droplets produced during tidal mouthbreathing. The human droplet emissions were directly conveyed to the OPC using a disposable mouthpiece, while a nose clip was used to prevent nasal breathing. One-way valve and High Efficiency Particulate Air (HEPA) filter were used to insure no ambient or exhaled particles were re-inhaled. The same experimental setup was used by Wurie et al<sup>55</sup> to characterize the emission of exhaled droplets from 188 tuberculosis-infected patients. With this large number of subjects and by using the OPC technique, Wurie et al were able to show that intrathoracic tuberculosis-infected patients produce significantly more bioaerosol than healthy subjects, in a particle size range that could transport *Mycobacterium tuberculosis*.

### 3.1.4 | Aerodynamic particle sizer

The Aerodynamic Particle Sizer (APS) evaluates the particle droplet aerodynamic diameter through the measure of the time of flight

of a particle being accelerated in a jet flow. The time of flight is "the time between two pulses of light scattered by the particle as it passes through two beams of light"<sup>42</sup> and depends on the capacity of the particle to accelerate, which permits to estimate the aerodynamic diameter of the particle. The typical size range of the APSs (TSI) used for the characterization of the particles is 0.5–20  $\mu\text{m}$ . The total airflow rate pumped through the APS is 5 L.min<sup>-1</sup> divided into 1 L.min<sup>-1</sup> of sampling airflow and 4 L/min of sheath flow.<sup>56</sup> The sheath flow is filtered and then rejoins the sampling flow rate. The total flow then passes through an accelerating nozzle, which induce a pressure loss and temperature drop of the gas surrounding the particle surface. The accelerated particle is thus submitted to a temperature difference with a high convective heat transfer coefficient, which usually produces evaporation of volatile particles. Therefore, the APS is considered as suitable for the analysis of solid particles and non-volatile droplets.<sup>56</sup> Morawska et al<sup>11</sup> designed a bench for the characterization of the exhaled droplets as discussed in Section 3.1.2 together with the droplets deposition analysis system, an APS was used for the droplets in the size range 0.5–20  $\mu\text{m}$ . The authors measured the diameter of the droplets at three different distances from the subject: 0, 100, and 300 mm. They found that the count median diameter inversely proportional to the distance from the subject, because of the equilibrium diameter changes with humidity. The same bench was used for another experimental study where both size distribution and humidity were measured at the abovementioned distances. They were able to distinguish different size distribution modes; droplets below 0.8  $\mu\text{m}$  were produced during all the exhalation activities at an average concentration of 0.75 part/cm<sup>3</sup>, a second mode at 1.8  $\mu\text{m}$  was also observed for all the activities at a concentration of 0.14 part/cm<sup>3</sup>.<sup>57</sup> Speaking produces two more modes, 3.5 and 5  $\mu\text{m}$  with a concentration of 0.04 and 0.16 part/cm<sup>3</sup>, respectively. They investigated the droplets evaporation through measuring the size distribution of droplets at different ages. As it was not technically possible to follow a single particle and measure the change of diameter due to evaporation, they assumed that measuring the droplet size distribution at different distances would be equivalent to measuring the size distribution of droplet at different ages. They used an APS at two different distances from the subject. The drying time for the droplets in the detectable size range of the APS was comparable to the drying time of pure water droplets, they evaporate in 0.8 seconds at 97% relative humidity, which made it technically difficult to detect the non-equilibrium evaporation.

Using an alternative technique, Yang et al measured the size distribution of the initial droplets using an APS. The exhaled breath was collected in a sample bag and to avoid droplet evaporation, the humidity inside the sample bag was maintained at 95%. They found that the average size distribution of cough droplets was in the range of 0.62–15.9  $\mu\text{m}$ . The APS has fine size intervals and a high sampling frequency,<sup>21,42</sup> which make it suitable for quantifying particles dispersion. Fang et al<sup>58</sup> used the APS to examine the decay of the size and concentration of the droplets along the main dispersion axis, and they found that this decay is exponential. Liu and Novoselac<sup>21</sup> also used the APS to measure the dry residues concentration in the breathing zone of a receiver manikin. A recent study by Asadi et al<sup>59</sup> used the APS

to analyze the effect of the voice loudness and the spoken language on the amount and size distribution of droplets emitted during speaking. The subjects were seated inside a hood with laminar ventilation, and a fennel was placed near the subject face to collect the emitted droplets. A distance between the subject face and the fennel was kept allowing a free flow of air into the fennel. In this study, the estimated evaporation time of the droplets was much less than the travelling time between the subject mouth and the measurement point in the APS. In this experiment, the subjects spoke the four world most spoken languages, and the APS was used to compare the concentration of sampled air. The authors found a positive correlation between the particle emission and the loudness of vocalization, regardless of the language spoken. Asadi et al<sup>60</sup> used the same experimental setup to analyze the effect of voice articulation on the particle emission rate. They were able to identify phones with higher droplets generation as well as observing that the number of emitted particles is proportional to the vowel content of the sentences.

He et al<sup>61</sup> conducted a detailed study on the droplet emissions from wind instruments using APS measurements. Based on a comparison of the aerosol production from a wide range of wind instruments with that of normal breathing and speaking, they classified the instruments into three risk categories: low (eg, tuba), intermediate (eg, clarinet), and high risk (eg, trumpet).

### 3.1.5 | Other techniques

In addition to the techniques mentioned above, there are a few less frequently used techniques. Loudon and Roberts<sup>45</sup> tried to directly observe with a microscope the dry residues collected on a filter at the outlet of the box described in Section 3.1.2 to collect the dry residues suspended in the air, inside the box. Authors observed that dry residues under 1  $\mu\text{m}$  were not detectable although the lower detection limit of the microscope was 0.5  $\mu\text{m}$ .

The Electrical Low-Pressure Impactor (ELPI, Dekati LTD) was used by Hersen et al<sup>62</sup> for the characterization of the size distribution of the cough dry residues produced by volunteers infected by influenza virus. The ELPI provides a real-time determination of the droplets aerodynamic diameter in the size range of 0.007–10  $\mu\text{m}$ , classified into 12 size intervals. Hersen et al collected the exhaled breath through a ventilated hood where the head of volunteers was placed. It is important to notice that when using such kind of hoods, the droplets interact with the ventilation flow rate depending on their size. Therefore, the ventilation flow rate and the sampling point should be well studied. ELPI enables real-time measurements of the size distribution which helps in studying the exhaled breath of a great number of volunteers, 78 individuals in Hersen et al.<sup>62</sup>

The Scanning Mobility Particle Sizer (SMPS) was another measurement technique that was used by Yang et al<sup>63</sup> to measure the fine dry residues of the droplets generated by coughing. The particle size range of the SMPS is 0.02–0.6  $\mu\text{m}$ . In this study, Yang et al SMPS has used in addition to APS to cover a wider size range, but almost no particles were observed in the size range of the SMPS.

### 3.2 | Non-intrusive measurement techniques

Non-intrusive measurement techniques have been developed during the course of the last two decades. Most of these techniques are used to determine the size distribution of the exhaled droplets. Using a non-intrusive technique eliminates the bias due to physical phenomena such as evaporation and condensation during the sampling process. This makes these non-intrusive techniques particularly suitable for measuring the initial droplets size distribution and for studying the evaporation process. Moreover, some non-intrusive techniques are used to measure the velocity and size of the droplets at different positions in the exhaled jet.

#### 3.2.1 | High-speed photography

High-speed photography technique was previously discussed in Section 2.1.1 for the characterization of the exhaled jet gas phase, through capturing images of tracer particles. This technique is also used to characterize the exhaled droplet dispersion. Zhu et al<sup>26</sup> studied the transport of droplets produced by coughing. To visualize the transport of the saliva droplets, the subjects' mouths were covered with flour and then the dispersion of the saliva droplets with flour particles was analyzed. The study showed that the droplets travel with high velocity during the first 30 cm. Then, the droplets velocity decreases and the maximum observed travel distance in this study was 2 m. Despite the role of the flour in visualizing the saliva droplets, the presence of this flour might affect the evaporation of the droplets and hence their dispersion. Nishimura et al<sup>64</sup> claimed to be the first to study the dynamics of the droplets expelled during coughing and sneezing. They developed a digital high-vision, high-speed video system to capture the movement of the droplets. A PIV image processing software was employed to track the brightness signal of the captured images and the obtained data are represented in a form of velocity vectors. Using this technique, they found that the initial average velocity of cough droplets of two subjects was 5 m/s, and after 84 cm these droplets lost their momentum. When considering sneezing, they determined corresponding values of 6 m/s and 30 cm, only. This measurement technique does not provide information about the droplet size. Bourouiba et al<sup>20</sup> also used this measurement technique based on high-speed photography of exhaled droplets. Through streak imaging technique, they were able to produce a picture of the droplets' trajectory, showing that large droplets follow a ballistic path depending on their size while small droplets followed the turbulent airflow. The minimum detectable droplet size depends on the performance of the optical setup and the digital camera.

#### 3.2.2 | Digital inline holography

In contrary to normal photography that affords only an image of intensity variations, holography records light phase which results in the production of 3D pictures. In conventional holography, a beam

from a coherent light source or laser is split into two beams; one illuminating the object itself and the other providing a reference. The object-illuminating beam is recombined, after being reflected by the body, with the reference beam which creates a phase interference that is registered onto the hologram plate. To retrieve the object, the plate is lit by a coherent light beam identical to the reference beam used at the recording of the hologram. It permits 3D viewing of the original object exactly as registered with all its optical information retrieved, but topographical or vertical measurements are yet possible.

In Digital Inline Holography (DIH), recently developed, the same phase interference concept is used to register holographic images using a digital camera. The camera then feeds the information into a computer program that numerically reconstructs the images. The numerical reconstruction process permits immediate quantitative access to the intensity and phases of topographic measurements accurate down to the nanometric scale. However, there is always a compromise between the measurement scale and measurement volume.

Shao et al<sup>65</sup> used the DIH to measure the shape, size, and concentration of the droplet generated during breathing. The DIH used system detects particles and droplets in the range of 0.5–50  $\mu\text{m}$ . The particle concentration was 170 part/L, and the average size was 1.7  $\mu\text{m}$  at 1.5 cm from the subject's mouth. Shao et al observed irregular particle shapes in addition to well-rounded droplets. By defining a roundness threshold, the authors estimated that 33% of the particles emitted at a distance of 1.5 cm are not droplets.

#### 3.2.3 | Laser measurement techniques based on Mie theory

The laser measurement techniques relying on Mie theory are non-intrusive techniques that are based on the measurement of the amount of light scattered by the droplets. For the characterization of the exhaled droplets, Chao et al<sup>27</sup> developed a device using this technique named Interferometric Mie Imaging (IMI) to measure the size distribution and the concentration of the droplets produced during coughing and speaking. IMI produced de-focused images of the droplets using a combination of a high-speed camera and laser sheet. The droplet diameter is obtained from the spatial frequency of the fringes in the image using geometrical analysis. The measurements were conducted at a distance of 10 and 60 mm from the mouth and the data were analyzed to consider the evaporation. Chao et al found that the geometric mean diameter for coughing and speaking are 13.5 and 16.0  $\mu\text{m}$ , respectively. The results obtained with the IMI showed good agreement with previous studies from Duguid<sup>43</sup> and Loudon & Roberts.<sup>45</sup> However, the measurement volume of the IMI system is about 60 mm<sup>3</sup>, which is much smaller than the total exhaled air volume. Thus, these results are insufficient to provide information about the total droplet number or droplet concentration. To overcome this limitation, Chao et al used

two estimation methods. The first estimation method was to divide the total volume of droplets by the size distribution obtained by IMI. The disadvantage of this method is the lack of information about the total droplet volume, as only two studies characterized the size of the droplets using collection instead of sampling techniques.<sup>43,45</sup> The second method was to obtain the droplet concentration by dividing the number of the sampled droplets over the IMI measurement volume. Calculating the droplet concentration using this second method assumes a uniform droplet concentration over the whole expelled air volume. This assumption could be confirmed by conducting IMI measurements at different locations covering a larger flow cross-sectional area.

This technique was also used to study the droplet dispersion in different environments. Chao and Wan<sup>66</sup> used this technique to validate a numerical model that compares the effect of two ventilation systems on the droplet dispersion, unidirectional downward and ceiling-return ventilation. The measurements were conducted in a Class 100 cleanroom where the supply air is vented through the roof toward a perforated-tiles floor to maintain the room at 21°C and 55% RH. A PIV system was used to capture the flow patterns and turbulence intensity inside the room while the size measurement of the cough-like droplets was performed by using Interferometric Mie Imaging (IMI) technique. The study demonstrated that the droplet of  $\leq 45 \mu\text{m}$  diameter dried out before deposition or extraction by ventilation system while the large droplet,  $\geq 87.5 \mu\text{m}$ , settle down before complete evaporation.

Laser particle size analyzer is another device that is based on the Mie theory. In this technique, a laser beam is used to illuminate a control volume that can contain multiple droplets, and the angular variation in the intensity of scattered light is directly related to the droplet diameter. The distribution of the sneezing droplets was studied by Han et al<sup>67</sup> using a laser particle size analyzer with a wide size range 0.1–1000  $\mu\text{m}$ . Han et al found that the geometrical mean of the unimodal distribution is 360.1  $\mu\text{m}$  (SD = 1.5) and 74.4  $\mu\text{m}$  for bimodal distribution (SD = 1.7). Another study by Zayas et al<sup>68</sup> also used the laser particle analyzer to measure the size distribution and concentration of the coughing droplets from 54 healthy subjects. The size range of the analyzer was 0.1–900  $\mu\text{m}$  divided into 60 size intervals. Despite the size range difference when compared to the OPC, Zayas et al concluded that 97% of measured particles have diameters lower than 1 micron, which is in accordance with values obtained by OPC. Although this technique is capable of measuring the large droplets diameter, in this experiment the distance between the mouth subject and the center of the measurement volume was 17 cm. Given the normal room conditions, evaporation effect cannot be ignored over this distance, which might explain the predominance of submicronic particles.

### 3.3 | Comment on disease transmission

This paper is divided into two parts, namely airflow and droplets characterization. However, when considering airborne disease transmission, the interaction of the droplets with the airflow is a crucial issue.

Table 1 lists all the experimental measured parameters for human breathing, coughing, speaking, and sneezing. These parameters contain boundary and initial flow conditions such as temperature, humidity, initial velocity, and mouth/nose area which are essential for modeling. Other measured parameters characterize the propagation of the flow which is of particular interest when analyzing the host-to-host transmission route. However, the relation between airflow propagation and airborne disease transmission is not direct as the viability of the pathogens depends not only on the flow characteristics but also on the type of the pathogen. Moreover, a recent study by Bourouiba et al<sup>69</sup> using high-speed photography shows that the average flow parameters are not sufficient to study the droplet-flow interaction. Instead, the flow structure contains vortices that entrain droplet clusters in warm and moist gas clouds. Bourouiba et al report that the effect of this gas cloud can extend the lifetime of the droplets expelled during coughing up to 1000 times and the droplets travel up to 7–8 m from the source. This distance varies significantly from air propagation distance shown in Table 1, which highlights the necessity for more quantitative measurement on the exhaled droplets motion and evaporation.

## 4 | CONCLUSION

In our review, we classified the exhaled airflow measurements techniques into two categories: global flow-field measurements, and pointwise measurements. Three global flow-field measurement techniques were identified, namely the high-speed photography, schlieren photography and Particle Image Velocimetry (PIV). These techniques provide information on the whole flow field and helps understanding the interactions between the exhaled flow, the thermal plume and the room airflow. The high-speed photography and the schlieren photography were applied to study the flow shape and its propagation into the space while the PIV was applied where detailed quantitative data of the velocity field was required. The pointwise measurements were used to measure the initial temperature, initial humidity, and velocity. To identify the points at which pointwise measurements should be conducted, one of the global flow-field measurement technique often precedes pointwise measurements. In the experiments where PIV measurements were applied to characterize the velocity field from human sources, the confinement effect due to the dimension of the box containing the tracer particles should be considered. The interpretation of measurement results should consider the applied measurement technique: This was clear for the propagation distance values found in literature, as values obtained by the schlieren photography were higher than those determined by the pointwise measurements.

The second part of the article summarizes the techniques applied for the characterization of the exhaled droplets and dry residues. These techniques can be used to determine three important parameters: droplet or dry residues sizes distribution, droplet velocity distribution, and travelled distance. Apart for three articles, all the reviewed articles in this section measured the size distribution of the droplets and/or the dry residues. Solid impaction, droplet



deposition analysis, optical particle counter, aerodynamic particle sizer, electrical low-pressure impactor scanning Mobility Particle Sizer, Liquid impingers, and filtration are the techniques used to measure the size distribution of the dry residues. Depending on the measurement principle, some correlation between the initial droplet diameter and the dry residues diameter could be applied to estimate the initial size of the droplets.

The evolution of the droplet size is important to study the transmission of the airborne diseases. It controls the droplet dynamics and determines the physical history of the living microorganisms transported in droplets. Limited experimental data are available to validate the evaporation models used in the analysis of the deposition and dispersion of the exhaled droplets. The used evaporation models<sup>70-72</sup> are validated versus experimental data obtained from a freefall evaporating droplet<sup>73</sup> or a stagnant droplet.<sup>74</sup> Despite the capability of IMI technique and Laser particle size analyzer in tracking the size evolution and velocity of the droplets over distance, only one single study applied IMI to trace droplets size and velocity over distance.<sup>66</sup> In addition, the Phase Doppler Anemometry technique, which is used in other applications to track the size and velocity of droplets over distance,<sup>75</sup> could also be used to track the droplets inside the human exhaled jet.

#### AUTHOR CONTRIBUTION

**Khansa Mahjoub Mohammed Merghani:** Conceptualization-Equal, Writing—original draft-Lead; **Benoit Sagot:** Conceptualization-Equal, Writing—original draft-Equal; **Evelyne Géhin:** Conceptualization-Equal, Writing—review and editing-Lead; **Guillaume Da:** Writing—review and editing-Supporting; **Charles Motzkus:** Writing—review and editing-Supporting.


#### PEER REVIEW

The peer review history for this article is available at <https://publons.com/publon/10.1111/ina.12770>.

#### DATA AVAILABILITY STATEMENT

Data sharing is not applicable to this article as no new data were created or analyzed in this study.

#### ORCID

Khansa Mahjoub Mohammed Merghani  <https://orcid.org/0000-0002-6122-5831>

#### REFERENCES

- Morawska L, Milton DK. It is time to address airborne transmission of COVID-19. *Clin Infect Dis*. July 2020. July 6, 2020;71(9):2311-2313. <https://academic.oup.com/cid/advance-article/doi/10.1093/cid/ciaa939/5867798>. Accessed July 16, 2020.
- Bahl P, Doolan C, de Silva C, Chughtai AA, Bourouiba L, MacIntyre CR. Airborne or droplet precautions for health workers treating coronavirus disease 2019? *J Infect Dis*. April 16, 2020;jiaa189. <https://academic.oup.com/jid/advance-article/doi/10.1093/infdis/jiaa189/5820886>. Accessed July 17, 2020.
- Li Y, Qian H, Hang J, et al. Evidence for probable aerosol transmission of SARS-CoV-2 in a poorly ventilated restaurant. *Infect Dis* (except HIV/AIDS). April 22, 2020. <http://medrxiv.org/lookup/doi/10.1101/2020.04.16.20067728>. Accessed July 16, 2020.
- Miller SL, Nazaroff WW, Jimenez JL, et al. Transmission of SARS-CoV-2 by inhalation of respiratory aerosol in the Skagit Valley Chorale superspreading event. *Indoor Air*. 2020. <http://dx.doi.org/10.1111/ina.12751>
- Chan J-W, Yuan S, Kok K-H, et al. A familial cluster of pneumonia associated with the 2019 novel coronavirus indicating person-to-person transmission: a study of a family cluster. *Lancet*. 2019;2020(395):514-523.
- Zhang J, Tian S, Lou J, Chen Y. Familial cluster of COVID-19 infection from an asymptomatic. *Critical Care*. 2020;24(1):119. <http://dx.doi.org/10.1186/s13054-020-2817-7>
- Sun Y, Tian L, Du X, Wang H, Li Y, Wu R. Epidemiological and clinical characteristics of a familial cluster of COVID-19. *Epidemiol Infect*. 2020;148:e145. [https://www.cambridge.org/core/product/identifier/S0950268820001521/type/journal\\_article](https://www.cambridge.org/core/product/identifier/S0950268820001521/type/journal_article). Accessed September 17, 2020
- Li Y-K, Peng S, Li L-Q, et al. Clinical and transmission characteristics of Covid-19 – a retrospective study of 25 cases from a single thoracic surgery department. *Curr Med Sci*. 2020;40:295-300.
- Ong SWX, Tan YK, Chia PY, et al. Air, surface environmental, and personal protective equipment contamination by severe acute respiratory syndrome coronavirus 2 (SARS-CoV-2) from a symptomatic patient. *JAMA*. 2020;323:1610.
- van Doremalen N, Bushmaker T, Morris DH, et al. Aerosol and surface stability of SARS-CoV-2 as compared with SARS-CoV-1. *N Engl J Med*. 2020;382:1564-1567.
- Morawska L, Johnson G, Ristovski Z, et al. Droplets Expelled during Human Expiratory Activities and their Origin. In Olesen BW, Toftum J, Wargocki P, Zukowska D, & Strom-Tejsten P eds. *Proceeding of the 11th International Conference on Indoor Air Quality and Climate Change*. (pp. 1-8). Denmark: University of Denmark; 2008.
- Siegel JD, Rhinehart E, Jackson M, Chiarello L. 2007 guideline for isolation precautions: preventing transmission of infectious agents in health care settings. *Am J Infect Control*. 2007;35:S65-S164.
- Melikov AK. Human body micro-environment: the benefits of controlling airflow interaction. *Build Environ*. 2015;91:70-77.
- Gupta JK, Lin C-H, Chen Q. Flow dynamics and characterization of a cough: flow dynamics and characterization of a cough. *Indoor Air*. 2009;19:517-525.
- Gupta JK, Lin C-H, Chen Q. Characterizing exhaled airflow from breathing and talking. *Indoor Air*. 2010;20:31-39.
- Xu C, Nielsen PV, Liu L, Jensen RL, Gong G. Human exhalation characterization with the aid of schlieren imaging technique. *Build Environ*. 2017;112:190-199.
- Tang JW, Nicolle AD, Klettner CA, et al. Airflow dynamics of human jets: sneezing and breathing – potential sources of infectious aerosols. Subbiah E, ed. *PLoS One*. 2013;8:e59970.
- Tang JW, Liebner TJ, Craven BA, Settles GS. A schlieren optical study of the human cough with and without wearing masks for aerosol infection control. *J R Soc Interface*. 2009;6:S727-S736.
- Kwon S-B, Park J, Jang J, et al. Study on the initial velocity distribution of exhaled air from coughing and speaking. *Chemosphere*. 2012;87:1260-1264.
- Bourouiba L, Dehandschoewercker E, Bush JWM. Violent expiratory events: on coughing and sneezing. *J Fluid Mech*. 2014;745:537-563.
- Liu S, Novoselac A. Transport of airborne particles from an unobstructed cough jet. *Aerosol Sci Technol*. 2014;48:1183-1194.
- Höppe P. Temperatures of expired air under varying climatic conditions. *Int J Biometeorol*. 1981;25:127-132.
- Tang JW, Nicolle A, Pantelic J, et al. Airflow dynamics of coughing in healthy human volunteers by shadowgraph imaging: an aid to aerosol infection control. Vijaykrishna D, ed. *PLoS One*. 2012;7:e34818.

24. Cao X, Liu J, Jiang N, Chen Q. Particle image velocimetry measurement of indoor airflow field: a review of the technologies and applications. *Energy Build.* 2014;69:367-380.
25. VanSciver M, Miller S, Hertzberg J. Particle image velocimetry of human cough. *Aerosol Sci Technol.* 2011;45:415-422.
26. Zhu S, Kato S, Yang J-H. Study on transport characteristics of saliva droplets produced by coughing in a calm indoor environment. *Build Environ.* 2006;41:1691-1702.
27. Chao CYH, Wan MP, Morawska L, et al. Characterization of expiration air jets and droplet size distributions immediately at the mouth opening. *J Aerosol Sci.* 2009;40:122-133.
28. Savory E, Lin WE, Blackman K, et al. Western cold and flu (WeCoF) aerosol study – preliminary results. *BMC Res Notes.* 2014;7:563.
29. Feng L, Yao S, Sun H, Jiang N, Liu J. TR-PIV measurement of exhaled flow using a breathing thermal manikin. *Build Environ.* 2015;94:683-693.
30. Jiang N, Yao S, Feng L, Sun H, Liu J. Experimental study on flow behavior of breathing activity produced by a thermal manikin. *Build Environ.* 2017;123:200-210.
31. Berlanga FA, Olmedo I, Ruiz de Adana M. Experimental analysis of the air velocity and contaminant dispersion of human exhalation flows. *Indoor Air.* 2017;27:803-815.
32. Mahajan RP, Singh P, Murty GE, Aitkenhead AR. Relationship between expired lung volume, peak flow rate and peak velocity time during a voluntary cough manoeuvre. *Br J Anaesth.* 1994;72:298-301.
33. Singh P, Mahajan RP, Murty GE, Aitkenhead AR. Relationship of peak flow rate and peak velocity time during voluntary coughing. *Br J Anaesth.* 1995;74:714-716.
34. Xu C, Nielsen PV, Gong G, Liu L, Jensen RL. Measuring the exhaled breath of a manikin and human subjects. *Indoor Air.* 2015;25:188-197.
35. Xu C, Nielsen PV, Gong G, Jensen RL, Liu L. Influence of air stability and metabolic rate on exhaled flow. *Indoor Air.* 2015;25:198-209.
36. Wells W. On air-borne infection: study II. Droplets and droplet nuclei. *Am J Epidemiol.* 1934;20:611-618.
37. Milton DK, Fabian MP, Cowling BJ, Grantham ML, McDevitt JJ. Influenza virus aerosols in human exhaled breath: particle size, culturability, and effect of surgical masks. *PLOS Pathog.* 2013;9:7.
38. Lindsley WG, Blachere FM, Thewlis RE, et al. Measurements of airborne influenza virus in aerosol particles from human coughs. Pekosz A, ed. *PLoS One.* 2010;5:e15100.
39. Fabian P, McDevitt JJ, DeHaan WH, et al. Influenza virus in human exhaled breath: an observational study. Fouchier RAM, ed. *PLoS One.* 2008;3:e2691.
40. Xie X, Li Y, Chwang ATY, Ho PL, Seto WH. How far droplets can move in indoor environments – revisiting the Wells evaporation-falling curve. *Indoor Air.* 2007;17:211-225.
41. Gralton J, Tovey E, McLaws M-L, Rawlinson WD. The role of particle size in aerosolised pathogen transmission: a review. *J Infect.* 2011;62:1-13.
42. Baron PA, Kulkarni P, Willeke K, eds. *Aerosol Measurement: Principles, Techniques, and Applications*, 3rd ed. Hoboken, NJ: Wiley; 2011.
43. Duguid JP. The size and the duration of air-carriage of respiratory droplets and droplet-nuclei. *J Hyg (Lond).* 1946;44:471-479.
44. Fennelly KP, Martyny JW, Fulton KE, Orme IM, Cave DM, Heifets LB. Cough-generated aerosols of *Mycobacterium tuberculosis*: a new method to study infectiousness. *Am J Respir Crit Care Med.* 2004;169:604-609.
45. Loudon RG, Roberts RM. Droplet expulsion from the respiratory tract. *Am Rev Respir Dis.* 1967;95(3):435-442. <https://doi.org/10.1164/arrd.1967.95.3.435>
46. Li Y, Chwang ATY, Ho PL, Seto WH, Yuen PL. Understanding droplets produced by nebulisers and respiratory activities. *Hong Kong Med J.* 2008;14:29-32.
47. Xie X, Li Y, Sun H, Liu L. Exhaled droplets due to talking and coughing. *J R Soc Interface.* 2009;6:S703-S714.
48. Johnson GR, Morawska L, Ristovski ZD, et al. Modality of human expired aerosol size distributions. *J Aerosol Sci.* 2011;42:839-851.
49. Fabian P, Brain J, Houseman EA, Gern J, Milton DK. Origin of exhaled breath particles from healthy and human rhinovirus-infected subjects. *J Aerosol Med Pulm Drug Deliv.* 2011;24:137-147.
50. Edwards DA, Man JC, Brand P, et al. Inhaling to mitigate exhaled bioaerosols. *Proc Natl Acad Sci.* 2004;101:17383-17388.
51. Holmgren H. *On the Formation and Physical Behaviour of Exhaled Particles.* Göteborg: Chalmers Univ. of Technology; 2011.
52. Almstrand A-C, Bake B, Ljungström E, et al. Effect of airway opening on production of exhaled particles. *J Appl Physiol.* 2010;108:584-588.
53. Papineni RS, Rosenthal FS. The size distribution of droplets in the exhaled breath of healthy human subjects. *J Aerosol Med.* 1997;10:105-116.
54. Wurie F, Polain LE, de Waroux O, et al. Characteristics of exhaled particle production in healthy volunteers: possible implications for infectious disease transmission. *F1000Research.* 2013;2:14.
55. Wurie FB, Lawn SD, Booth H, Sonnenberg P, Hayward AC. Bioaerosol production by patients with tuberculosis during normal tidal breathing: implications for transmission risk. *Thorax.* 2016;71:549-554.
56. *TSIModel 3321 Aerodynamic Particle Sizer Spectrometer Instruction Manual*; 109.
57. Morawska L, Johnson GR, Ristovski ZD, et al. Size distribution and sites of origin of droplets expelled from the human respiratory tract during expiratory activities. *J Aerosol Sci.* 2009;40:256-269.
58. Fang L, Lau A, Chan C, Hung C, Lee T. Aerodynamic properties of biohazardous aerosols in hospitals. *Hong Kong Med J.* 2008;14:26-28.
59. Asadi S, Wexler AS, Cappa CD, Barreda S, Bouvier NM, Ristenpart WD. Aerosol emission and superemission during human speech increase with voice loudness. *Sci Rep.* 2019;9:2348. December 2019. <http://www.nature.com/articles/s41598-019-38808-z>. Accessed February 18, 2020.
60. Asadi S, Wexler AS, Cappa CD, Barreda S, Bouvier NM, Ristenpart WD. Effect of voicing and articulation manner on aerosol particle emission during human speech. *PLOS ONE.* 2020;15(1):e0227699. <http://dx.doi.org/10.1371/journal.pone.0227699>
61. He R, Gao L, Trifonov M, Hong J. Aerosol generation from different wind instruments. *J Aerosol Sci.* 2021;151:105669.
62. Hersen G, Moularat S, Robine E, et al. Impact of health on particle size of exhaled respiratory aerosols: case-control study. *CLEAN Soil Air Water.* 2008;36:572-577.
63. Yang S, Lee GWM, Chen C-M, Wu C-C, Yu K-P. The size and concentration of droplets generated by coughing in human subjects. *J Aerosol Med.* 2007;20:484-494.
64. Nishimura H, Sakata S, Kaga A. A new methodology for studying dynamics of aerosol particles in sneeze and cough using a digital high-vision, high-speed video system and vector analyses. Harrod K, ed. *PLoS One.* 2013;8:e80244.
65. Shao S, Zhou D, He R, et al. Risk assessment of airborne transmission of COVID-19 by asymptomatic individuals under different practical settings. *J Aerosol Sci.* 2021;151:105661.
66. Chao CYH, Wan MP. A study of the dispersion of expiratory aerosols in unidirectional downward and ceiling-return type airflows using a multiphase approach. *Indoor Air.* 2006;16:296-312.
67. Han ZY, Weng WG, Huang QY. Characterizations of particle size distribution of the droplets exhaled by sneeze. *J R Soc Interface.* 2013;10:20130560.
68. Zayas G, Chiang MC, Wong E, et al. Cough aerosol in healthy participants: fundamental knowledge to optimize droplet-spread infectious respiratory disease management. *BMC Pulm Med.* 2012;12(1):11. December 2012. <https://bmcpulmed.biomedcentral.com/articles/10.1186/1471-2466-12-11>. Accessed March 3, 2019.
69. Bourouiba L. Turbulent gas clouds and respiratory pathogen emissions: potential implications for reducing transmission of COVID-19.

- JAMA. March 26, 2020;323(18):1837-1838. <https://jamanetwork.com/journals/jama/fullarticle/2763852>. Accessed July 19, 2020.
70. Chen C, Zhao B. Some questions on dispersion of human exhaled droplets in ventilation room: answers from numerical investigation. *Indoor Air*. 2010;20:95-111.
  71. Gao N, Niu J, He Q, Zhu T, Wu J. Using RANS turbulence models and Lagrangian approach to predict particle deposition in turbulent channel flows. *Build Environ*. 2012;48:206-214.
  72. Wei J, Li Y. Airborne spread of infectious agents in the indoor environment. *Am J Infect Control*. 2016;44:S102-S108.
  73. Kukkonen J, Vesala T, Kulmala M. The interdependence of evaporation and settling for airborne freely falling droplets. *J Aerosol Sci*. 1989;20:749-763.
  74. Liu L, Wei J, Li Y, Ooi A. Evaporation and dispersion of respiratory droplets from coughing. *Indoor Air*. 2017;27:179-190.
  75. Castanet G, Lebouché M, Lemoine F. Heat and mass transfer of combusting monodisperse droplets in a linear stream. *Int J Heat Mass Transf*. 2005;48:3261-3275.

**How to cite this article:** Mahjoub Mohammed Merghani K, Sagot B, Gehin E, Da G, Motzkus C. A review on the applied techniques of exhaled airflow and droplets characterization. *Indoor Air*. 2021;31:7-25. <https://doi.org/10.1111/ina.12770>